# ADVANCING FOREST ABOVEGROUND BIOMASS MAPPING BY INTEGRATING GEDI WITH OTHER EARTH OBSERVATION DATA USING A CLOUD COMPUTING PLATFORM: A CASE STUDY OF ALABAMA, UNITED STATES.

Janaki Sandamali[a]* and Lana L. Narine[a]

College of Forestry, Wildlife and Environment, Auburn University, Auburn, AL 36849, USA

*jsk0043@auburn.edu

This manuscript is currently a preprint and is scheduled for submission to a scientific journal shortly. As part of the peer-review process, both the structure and content of this manuscript may undergo revisions. Upon acceptance, the final version of this manuscript will be accessible through the 'Peer-reviewed Publication DOI' link provided on this webpage.

**Advancing forest aboveground biomass mapping by integrating GEDI with other Earth Observation data using a cloud computing platform: A case study of Alabama, United States.**


## Abstract

Forest aboveground biomass (AGB) is a crucial indicator for monitoring carbon and requires accurate quantification. This study aimed to advance AGB estimation using open access Earth observation (EO) data and cloud computing, focusing on Alabama, USA. The specific objectives were to: (1) develop a workflow for creating a 30 m forest AGBD map with GEDI, using GEE, (2) evaluate and compare GEDI-derived maps from ecoregion-specific models with estimates derived from a generalized modeling approach, and (3) compare GEDI-derived AGBD map with existing field inventory data and global AGB product. Utilizing GEE, GEDI footprint-level (~25 m diameter) AGBD was extrapolated with EO and ancillary data by employing random forest machine learning. Two estimation approaches were assessed: statewide and ecoregion-specific models for Alabama's six ecoregions. Ecoregion models showed superior accuracy ($R^2$: 0.34–0.73; RMSE: 49.09–53.78 Mg/ha) compared to the statewide model ($R^2$: 0.32; RMSE: 70.48 Mg/ha). Validation with Forest Inventory and Analysis data and the European Space Agency Climate Change Initiative AGBD yielded $R^2$ of 0.50 and 0.81, and RMSE of 33.95 Mg/ha and 83.12 Mg/ha, respectively. The study underscores the importance of ecoregion-specific modeling and demonstrates the potential of open-access EO data and platforms in advancing AGB estimation.


## 1. Introduction

Forests play a crucial role in the Earth's carbon cycle, constituting around 30% of the planet's total area and storing nearly 45% of its carbon reserves (Bonan, 2008, Rodríguez-Veiga et al., 2017). Aboveground biomass (AGB) serves as a pivotal indicator for assessing forest carbon stocks (Yang et al., 2023). Forest of the Southern United States (US) stand out as comprising of one of the world's most productive timberland systems (Shephard et al., 2022). Among them, Alabama holds the third-largest commercial forestland in the US with over 23 million acres of forest lands covering almost 70% of the state (Duncan, 2013). Further, Alabama's forests are estimated to store approximately 1.16 billion metric tons of carbon (AFC, 2020). AGB stands as a crucial indicator of carbon and its dynamic nature necessitates continuous measurement over time for accurate carbon estimation. Traditional field surveys carried out by forestry experts yield accurate forestry information. Field-based methodologies are time-consuming, labor-intensive, and may be cost prohibitive, and compounded by accessibility challenges in regions featuring steep slopes (Cao, 2022). Hence, remote sensing, and particularly spaceborne light detection and ranging (lidar), have emerged as powerful tools for assessing forest structure and estimating AGB over large areas with remarkable detail (Harris et al., 2021, Hummel et al., 2011, Nandy et al., 2021).

The Global Ecosystem Dynamics Investigation (GEDI) is a high-resolution spaceborne lidar instrument designed specifically to retrieve vegetation structure (Dubayah et al., 2022). Launched in 2018, GEDI, stationed on the International Space Station, offers measurements of forest vertical structure in temperate and tropical regions between 51.6° N and S latitude. GEDI offers both footprint and gridded products, encompassing raw and geolocated waveforms, footprint-level canopy height and profile metrics, gridded canopy height metrics and variability, along with footprint and gridded above ground biomass density (AGBD) (Dubayah et al., 2020, Dubayah et al., 2022, Kellner et al., 2022). The gridded AGBD (GEDI L4B) is provided at a 1 km resolution, while the footprint AGBD with a 25 m diameter (GEDI L4A) provides AGBD spaced roughly 60 m along-track and approximately 600 m apart across-track.

Spaceborne lidar inherently faces challenges such as the lack of continuous spatial coverage. Therefore, fusion with other Earth Observation (EO) data enables the spatiotemporal extrapolation which allow generation of continuous spatial coverage (Potapov et al., 2021, Aguilar et al., 2024). In this study, we considered a range of EO data representing various portions of the electromagnetic spectrum, as

suggested by previous studies, to represent a range of forest parameters. These datasets include Sentinel-1, Sentinel-2, Global 30 m digital elevation model (GLO30 DEM), Landsat 9, and LANDFIRE data (Arévalo et al., 2023, Guerra-Hernández et al., 2022, Nandy et al., 2021, Malambo et al., 2023b). An interesting aspect of our analysis is the incorporation of Landsat 9 and LANDFIRE data. This decision was driven by the limited number of studies exploring the utility of Landsat 9 for AGB estimation. Moreover, to our knowledge, none have integrated LANDFIRE in conjunction with Landsat 9 data for AGBD mapping.

Analysis with spaceborne lidar requires managing substantial and increasingly voluminous datasets, such as the billions of forest structural data sampler points provided by GEDI across the tropics (Holcomb et al., 2023). Integrating spaceborne lidar with other EO data, especially for larger areas, necessitates the management of extensive and growing volumes of lidar data (Béjar-Martos et al., 2022). Google Earth Engine (GEE) has emerged as a viable platform for this purpose, offering a comprehensive framework for effectively managing, sharing, and modeling spatial data (Gorelick et al., 2017, Kacic et al., 2021).

Considering the complexities of spectral variation within land cover classes and the challenges of per-pixel classification, a 30 m grid size has emerged as the preferred spatial resolution. This resolution effectively captures diverse features on Earth's surface while maintaining a balance between detail and coverage (Chen et al., 2015). Furthermore, when conducting regional-scale AGBD estimation, it is crucial to consider the inherent characteristics of vegetation of the region. As highlighted by CES (1997), ecoregions play a vital role in shaping regional environmental management assessments, reporting, and decision-making processes. Level III ecoregions, being smaller in scale, enable the identification of local characteristics and the formulation of more specifically oriented management strategies. Therefore, in this study, we considered a 30 m resolution and ecoregion-based approach when estimating AGBD.

The primary goal of this study is to advance AGB estimation using free and open EO data and a cloud-computing platform. The specific objectives of this study were to: (1) develop a workflow for creating a 30 m forest AGBD map with GEDI, using GEE, (2) evaluate and compare GEDI-derived maps from ecoregion-specific models with estimates derived from a generalized modeling approach, and (3) compare state-level GEDI-derived AGBD map with existing field inventory data and global AGB products.

## 2. Methodology

### 2.1 Study area

The state of Alabama, situated in the southeastern US between 30° and 35° north latitude and 85° to 88.5° west longitude, covers a total area of approximately 135,767 $km^2$ (Figure 1). Alabama boasts a diverse landscape, including mountains, mixed forests, and coastal plains. The predominant land use in the state is timberlands, constituting 71% of the total land area (Adjei et al., 2023). Alabama experiences a climate characterized by mild winters, hot summers, and consistent year-round precipitation. Renowned for its rich biodiversity, Alabama stands as one of the most ecologically diverse states in the United States, serving as a global hotspot for various plants and animal species (Duncan, 2013). The ecological composition of Alabama is categorized into six level III ecoregions: interior plateau, southwestern Appalachians, piedmont, southeastern plains, southern coastal plain, and ridge and valley as depicted in Figure 1 (d)*(AWF, 2008, USFWI, 2024)*.

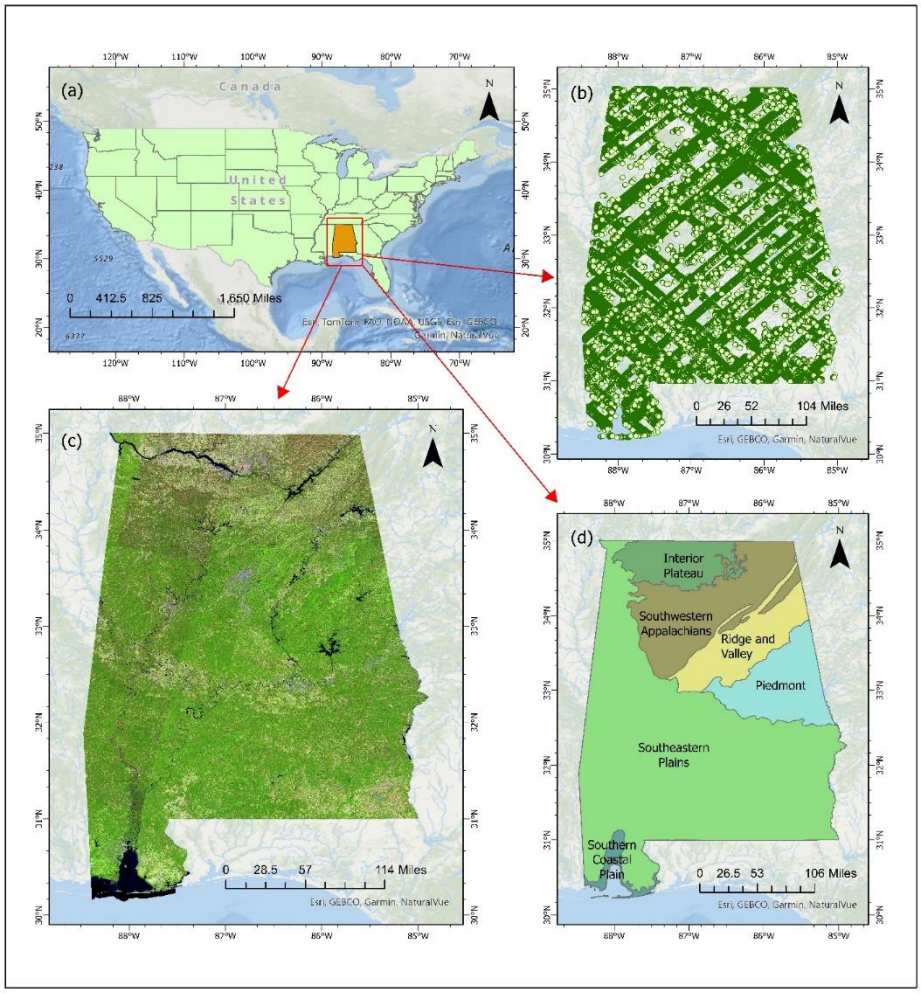


Figure 1. Study area of the investigation. (a) The spatial location of State of Alabama respect to the United States, (b) GEDI L4A footprint biomass data, (c) Landsat 9 False color (vegetative analysis) composite image (Bands: SWIR-1, Near Infra-red (NIR), Red), and (d) Level III ecoregions of the study area.

### 2.2 Data

The data employed in the study included open-access EO data obtained from various sources, including the Oak Ridge National Laboratory Distributed Active Archive Centre (ORNL DAAC), GEE catalog, LANDFIRE web portal, and Earth Resources Observation and Science Center.

#### 2.2.1. GEDI L4A Footprint Level Aboveground Biomass Density data

GEDI L4A acquired from January 1, 2022, to December 31, 2022, were downloaded from the ORNL DAAC. A comprehensive filtration process was conducted, guided by GEDI quality filters and previous studies, with a total of seven filters applied (Dubayah, 2022, Liu et al., 2021, Shendryk, 2022). Initially, data not meeting Level 4A quality requirements were excluded using the 'l4_quality_flag'. Subsequently, a beam sensitivity threshold of 0.98 was applied by considering Alabama's mixed forest characteristics, aiming to minimize measurement error in relative height metrics (Dubayah, 2022). Further refinement

involved the removal of unreliable GEDI measurements which exhibited more than 50% relative standard error as showed by Shendryk (2022). Additionally, GEDI measurements on slopes greater than 30 degrees were excluded, as prior findings indicated their adverse impact on the accurate retrieval of both terrain and tree heights (Liu et al., 2021). Then, GEDI data within unsuitable land cover and land use categories (e.g., built-up, barren, shrub/scrub, grasslands, etc.) were removed according to the National Land Cover Database (NLCD) (Shendryk, 2022). Then, GEDI measurements exclusively from the full power beams ('BEAM0101', 'BEAM0110', 'BEAM1000', and 'BEAM1011'), specifically designed for dense vegetation, were selected (Liu et al., 2021). Furthermore, GEDI data acquired during nighttime (solar elevation < 0) were utilized to mitigate the adverse effects of background solar illumination since waveform quality is compromised during daytime due to the impact of solar interference (Liu et al., 2021, Shendryk, 2022). Out of all available GEDI measurements (82,530,974), 812,195 (approximately 1%) remained after the data filtering for further processing as in Figure 2.

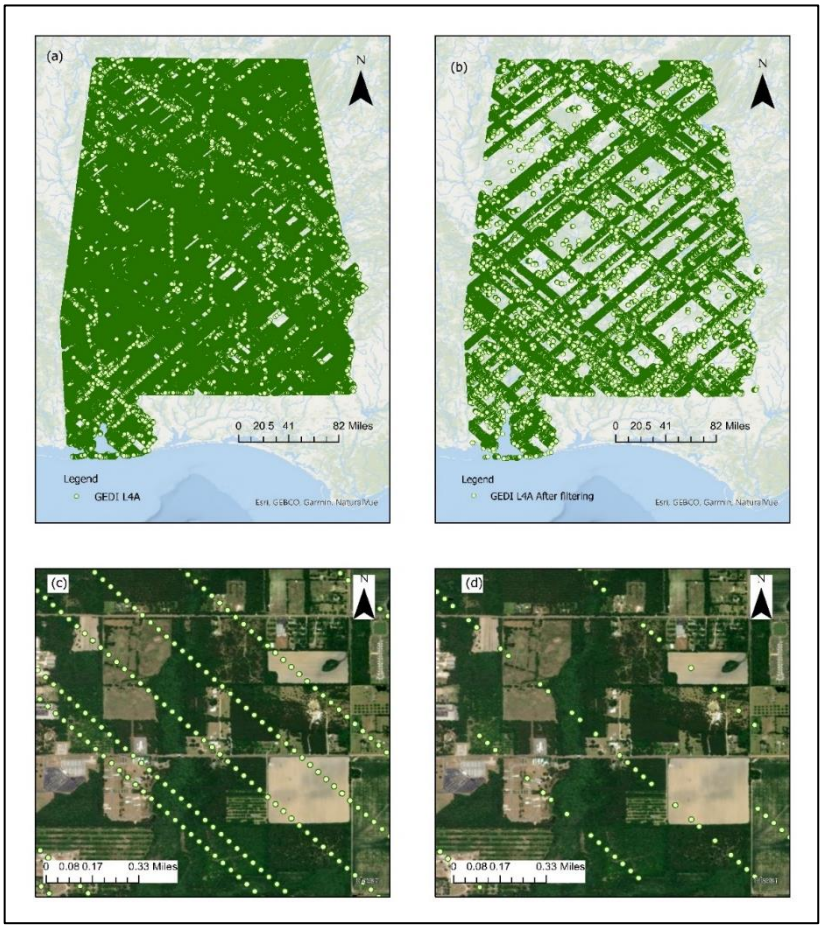


Figure 2. GEDI footprints over the State of Alabama for 2022 (a) Before filtering, (b) After filtering, (c) Zoomed area of showing the distribution of GEDI data over the selected study site before filtering for better representation with spatial distribution, (d) The same Zoomed area after filtering.

The distribution of GEDI L4A AGBD exhibited significant skewness, with values ranging from 0 Mg/ha to 3,730 Mg/ha. To prepare the data for analysis, various transformations were explored, including box cox, inverse, logarithmic, and square root transformations (Figure 3). After experimentation, the square root transformation was selected, as it rendered the distribution closer to a normal Gaussian distribution, enhancing the model's predictive accuracy and reducing bias (Shendryk, 2022). Subsequently, the transformed data was uploaded to GEE for further analysis, serving as the response variable in the model.

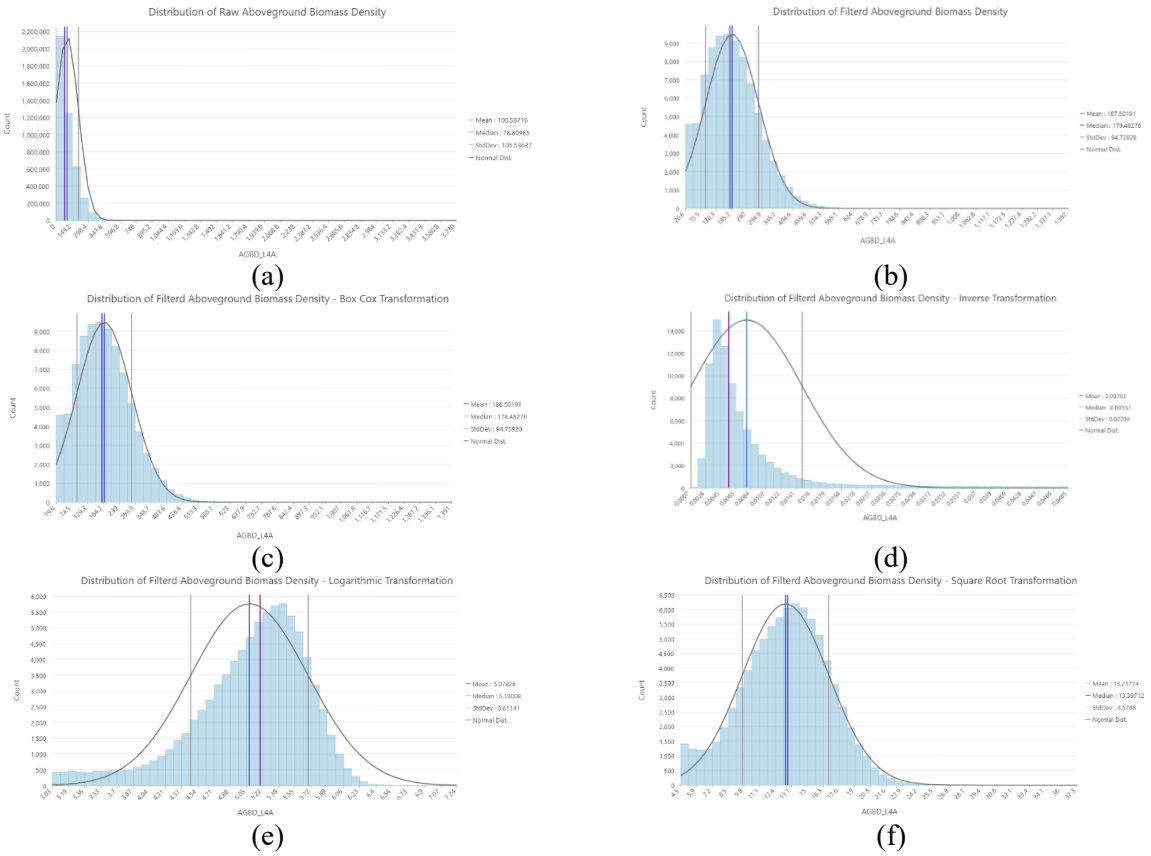


Figure 3. frequency distribution of GEDI L4A (a) The raw AGBD data, (b) filtered AGBD after applying filters to remove unsuitable erroneous footprint AGB, (c) Box Cox transformation, (d) Inverse transformation, (e) logarithmic transformation, (f) Square root transformation.

### 2.2.2. Mapped Earth Observation Predictors

Predictor variables used for upscaling footprint-level AGBD are listed in Table 1. Variables considered are deemed important in mapping AGB and forest structural parameters according to past literature.

Table 1. Data Sources and variables incorporated in the study for forest AGB estimation.

| No | Source | Variables | Reference |
|---|---|---|---|
| 01 | Sentinel-1 | VV / VH<br>band ratios (VV/VH)<br>band differences (VV - VH)<br>Textures<br>angular second moment, contrast, correlation, dissimilarity, entropy, variance, difference entropy, difference variance. | (Guerra-Hernández et al., 2022, Nandy et al., 2021, Li et al., 2020) |
| 02 | Sentinel-2 / Landsat 9 | Spectral bands: | (Madundo et al., 2023, Shendryk, 2022, Moradi et al., 2022, Jiang et al., 2022) |

| | | | |
|---|---|---|---|
| | | Near-infrared (Nir) / Red / Green / Blue / rededge1 / rededge2 / rededge3 / rededge4 / swir1 / swir2<br>Vegetation Indices:<br>Normalized Difference Vegetation Index (NDVI) / Ratio Vegetation Index (RVI) / Soil Adjusted Vegetation Index (SAVI) / Simple Ratio Vegetation Index (SR) / Optimized Soil Adjusted Vegetation Index (OSA) / Green Normalized Difference Vegetation Index (GNDVI) / Modified Soil Adjusted Vegetation Index (MSAVI) / Green Chlorophyll Index / green Chlorophyll Index (CI green) | |
| 03 | GLO30 DEM | DEM / Slope / Aspect | (Franks and Rengarajan, 2023) |
| 04 | LANDFIRE Data | Canopy Bulk Density (CBD), Canopy Base Height (CBH), Canopy Cover (CC), Canopy Height (CH), Existing Vegetation Cover (EVC), and Existing Vegetation Height (EVH) | (La Puma, 2023, Rollins, 2009, Malambo et al., 2023a). |
| 05 | NLCD Data | Land cover / Tree canopy cover | (Dewitz, 2023, Tiwari and Narine, 2022) |

2.2.2.1 Sentinel-1

The Sentinel-1 satellites collect C-band SAR, utilizing the Interferometric Wide Swath mode with VV (Vertical transmit - Vertical receive) and VH (Vertical transmit - Horizontal receive) polarizations, yielding Multi-Look Ground Range-Detected products (Laurin et al., 2018, ESA, 2012). All available Sentinel-1 images from January to December 2022 were utilized in this study, sourced from the 'COPERNICUS/S1_GRD' Sentinel-1 image collection within the GEE. These images were processed to backscatter coefficient ($\sigma^\circ$) in decibels (dB). For analysis, Sentinel-1 imagery was composited by computing the median of each band from all ascending orbit images at a spatial resolution of 30 m, and then mosaicked to cover the extent of Alabama. Additionally, band ratios (VV/VH) and band differences (VV - VH) were calculated, as they have demonstrated efficacy in forest-related studies, along with the VV and VH bands (Soudani et al., 2021). As shown by Chen et al. (2019) the texture features from Sentinel -1 data were more suitable for AGB estimation. Therefore, our study derived a range of textures from the Grey Level Co-occurrence Matrix (GLCM) using both VV and VH polarizations.

2.2.2.2 Sentinel-2

The Sentinel-2 data accessible in the GEE platform was obtained from scihub and processed using the Sen2Cor which is a processor for Sentinel-2 Level 2A product generation and formatting (esa, 2022). The study incorporated Sentinel data spanning from January 2022 to December 2022. Initially, atmospheric corrections were applied while simultaneously masking out clouds and cloud shadows from all images. This was achieved by utilizing the QA60 band, which contains quality assessment data, including information on cloud and cirrus presence. The bit 10 of the QA60 band evaluates cloud presence (0: absent, 1: present), while bit 11 assesses cirrus presence (0: absent, 1: present). Subsequently, bit masks for cloud and cirrus were detected and applied to mask out corresponding areas from the images. Data filtering was then performed, retaining only images with a cloud pixel percentage of less than five.

Following this, all images were composited by computing the median of all cloud and cloud shadow-masked images, with the resultant resolution set at 30 m (Shendryk, 2022). Moreover, Sentinel-2 imagery was employed to derive vegetation indices, which have previously shown adverse effects on AGB estimation, as illustrated in Table 1.

2.2.2.3 Landsat 9

Data from Landsat 9, accessible through the GEE, provides atmospherically corrected surface reflectance and land surface temperature measurements derived from OLI/TIRS sensors. These images include five visible and near-infrared bands, two short-wave infrared (SWIR) bands processed to orthorectified surface reflectance, one thermal infrared band processed to orthorectified surface temperature, along with quality assessment bands (Jiang et al., 2022). For our study, Landsat 9 images from January to December 2022 in Collection 2, Tier 1, Level 2 data were utilized, following additional processing to enhance geometric and radiometric accuracy. Cloud masking based on 'QA_PIXEL' values was applied, followed by filtering to retain images with less than five percent cloud cover. The images were then sorted in descending order to prioritize recent acquisitions, culminating in the computation of a median composite. Furthermore, Landsat 9 imagery was utilized to derive vegetation indices, which have previously shown significant impacts on AGB estimation, as depicted in Table 1.

2.2.2.4 GLO30 DEM

The GLO30 DEM, extracted from WorldDEM data acquired between 2011 and 2015, is publicly accessible via GEE and was subset to Alabama. Subsequently, slope and aspect calculations were performed to serve as predictor variables for analysis (Franks and Rengarajan, 2023).

**2.2.3. Other Ancillary Data**

2.2.3.1 LANDFIRE Data

LANDFIRE is an interagency initiative aimed at providing comprehensive biological, ecological, and geospatial data and databases covering the contiguous United States, Alaska, Hawaii, and insular areas (La Puma, 2023). It offers consistent and detailed maps and data delineating vegetation, wildland fuel, fire regimes, and ecological deviation from historical norms across the nation at a 30 m resolution. This study utilizes CBD, CBH, CC, CH, EVC, EVH all of which are appropriate to biomass and forest parameters as illustrated in Table 1.

2.2.3.2 NLCD Land Cover and Tree Canopy Datasets

The NLCD serves as an operational program for monitoring land cover in the United States, offering updated information spanning from 2001 to present (Dewitz, 2023). In our study, we utilized the NLCD 2021 land cover and tree canopy cover products from the U.S. Forest Service as an independent predictor variables in our estimation of AGBD (Dewitz, 2023, Tiwari and Narine, 2022).

**2.3 Extrapolating GEDI L4A and EO data to estimate AGBD.**

The methodology as depicted in Figure 4 involves collection of footprints AGBD from GEDI L4A, integration of multisource EO data and perform analysis in GEE. A total of 63 predictor variables, sourced from various platforms, were employed for estimating AGBD. These variables include 20 from Sentinel-1 derivatives, 18 from Sentinel-2, 14 from Landsat 9, three from GLO 30 DEM derivatives, six from the LANDFIRE program, and two from the NLCD. To assess the efficacy of our methodology, we adopted two modeling approaches: a statewide model treating the entire region as a single entity (hereafter

referred to as Model 1) and an ecoregion-specific model (hereafter referred to as Model 2). These models were trained using a random forests (RF) algorithm, a robust machine-learning technique for AGBD mapping, as proven by previous literature. (Narine et al., 2019, Nandy et al., 2021). The data was partitioned into 70% for model training and 30% for holdout testing. Finally, by considering holdout test data, US Forest Inventory and Analysis program (FIA) data, and European Space Agency (ESA) Climate Change Initiative (CCI) AGBD, we performed accuracy assessment and selected the best estimation model.

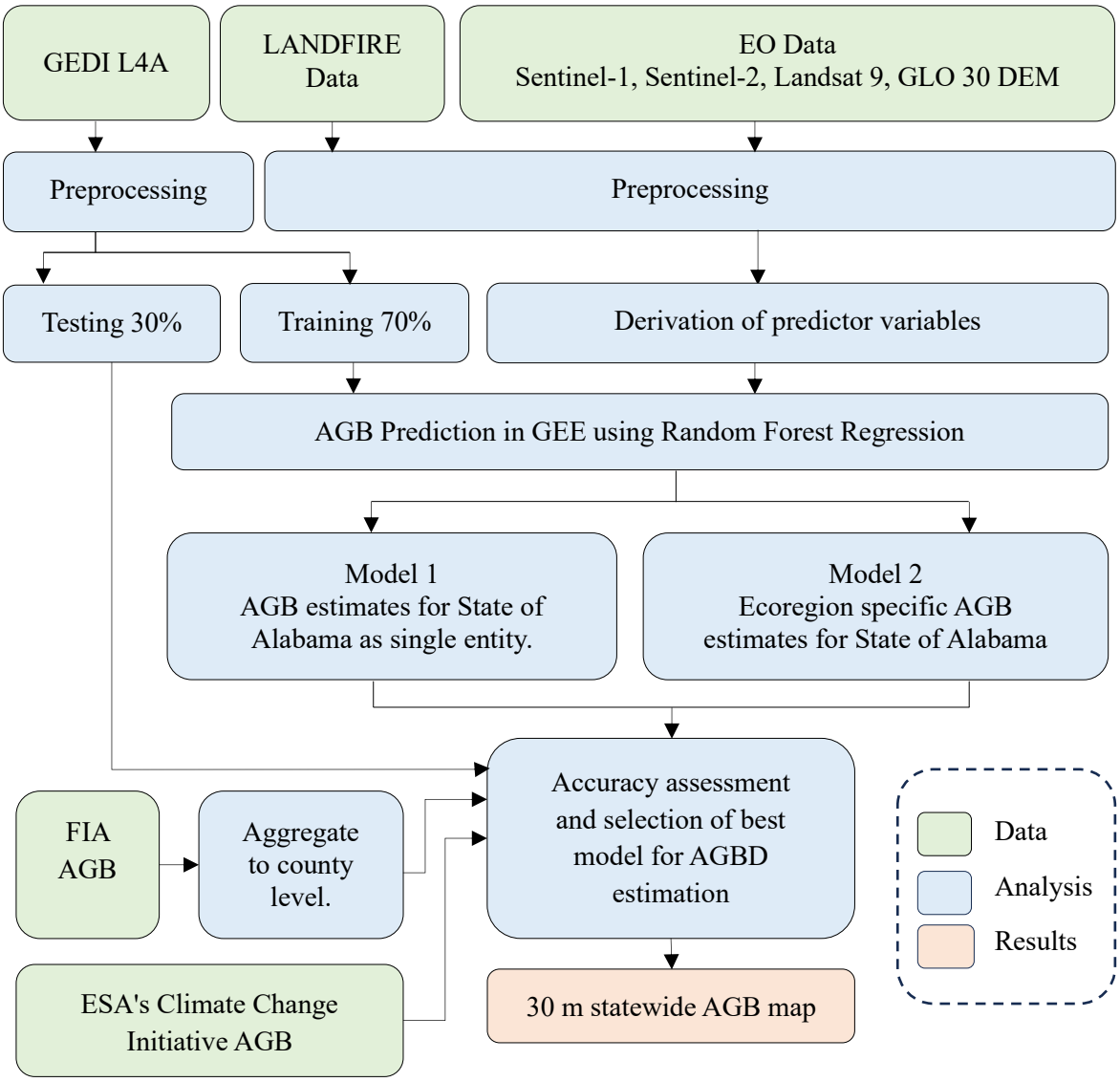


Figure 4. The workflow adopted in experimental analysis.

### 2.4 Validation of predicted AGBD

To assess accuracy, we employed two approaches. Initially, we utilized data obtained from the FIA program, spanning from 2013 to 2023, to minimize the temporal gap between estimated AGBD maps and FIA measurements. However, due to ecological integrity and security concerns, the accurate locations of

these plots are displaced by approximately one mile, making direct assessment of AGBD impractical. Consequently, we aggregated FIA plot data by computing the average AGBD at the county level for comparison, as illustrated in Figure 5. Subsequently, we obtained the average AGBD for each county from the estimated AGBD generated by our study and performed the comparison.

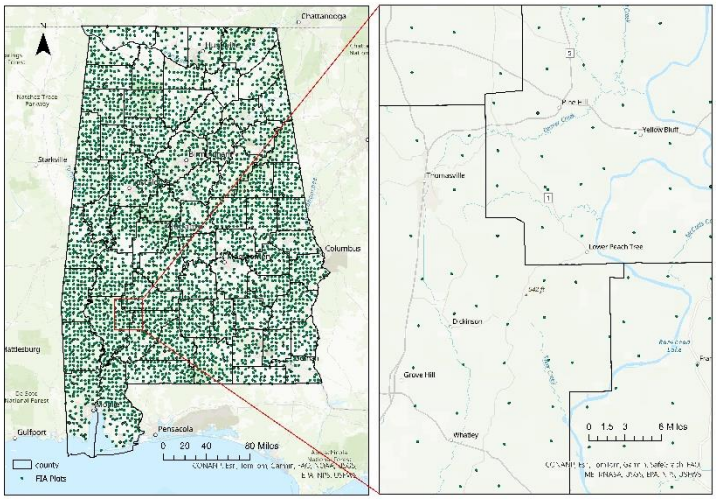


(a) (b)

Figure 5. Validation data (a) Distribution of 6071 FIA plots across 67 counties within the State of Alabama and (b) a detailed view of the aggregation process for deriving county-level averaged AGBD data.

Additionally, we utilized the ESA CCI AGBD dataset of 2020 as a secondary approach to the comparison (Figure 6). CCI map was masked to the geographic extent of the state of Alabama and re-projected to a uniform frame of reference (NAD 1983 Albers contiguous USA) and then performed pixel-by-pixel comparison.

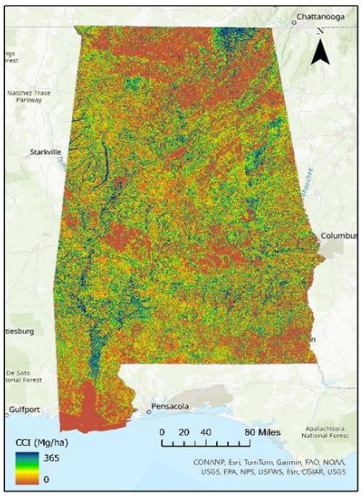


Figure 6. CCI AGBD product for 2020 at a spatial resolution of 100 m.

Finally, we computed statistical values to assess the accuracy of the estimated AGB from the study. These statistical measures encompassed: (i) the coefficient of determination ($R^2$), (ii) adjusted $R^2$, (iii) the root-mean-square error (RMSE), and (iv) the relative RMSE (rRMSE).

## 3. Results

### 3.1 Accuracy assessment through withheld test data.

As depicted in the Figure 6 the accuracy metrics produced using withheld test data indicate superior performance of models 2 ($R^2$ = 0.22-0.72, RMSE: 2.53 Mg/ha - 1.80 Mg/ha, rRMSE = 23.39 -13.39) compared to model 1 ($R^2$ = 0.42, RMSE: 2.72 Mg/ha, rRMSE = 20.60). Notably, the model 2 exhibited varied $R^2$ and RMSE values across different ecoregions, with the southern coastal region showing suboptimal performance ($R^2$: 0.22, RMSE: 2.53 Mg/ha, RRMSE: 23.39%), primarily attributed to insufficient *N* (number of samples) for analysis and the inherent characteristics of the land cover which includes estuaries, salt marshes, lagoons, bayous, river deltas, and wetlands (USFWI, 2024, Bouasria et al., 2023).

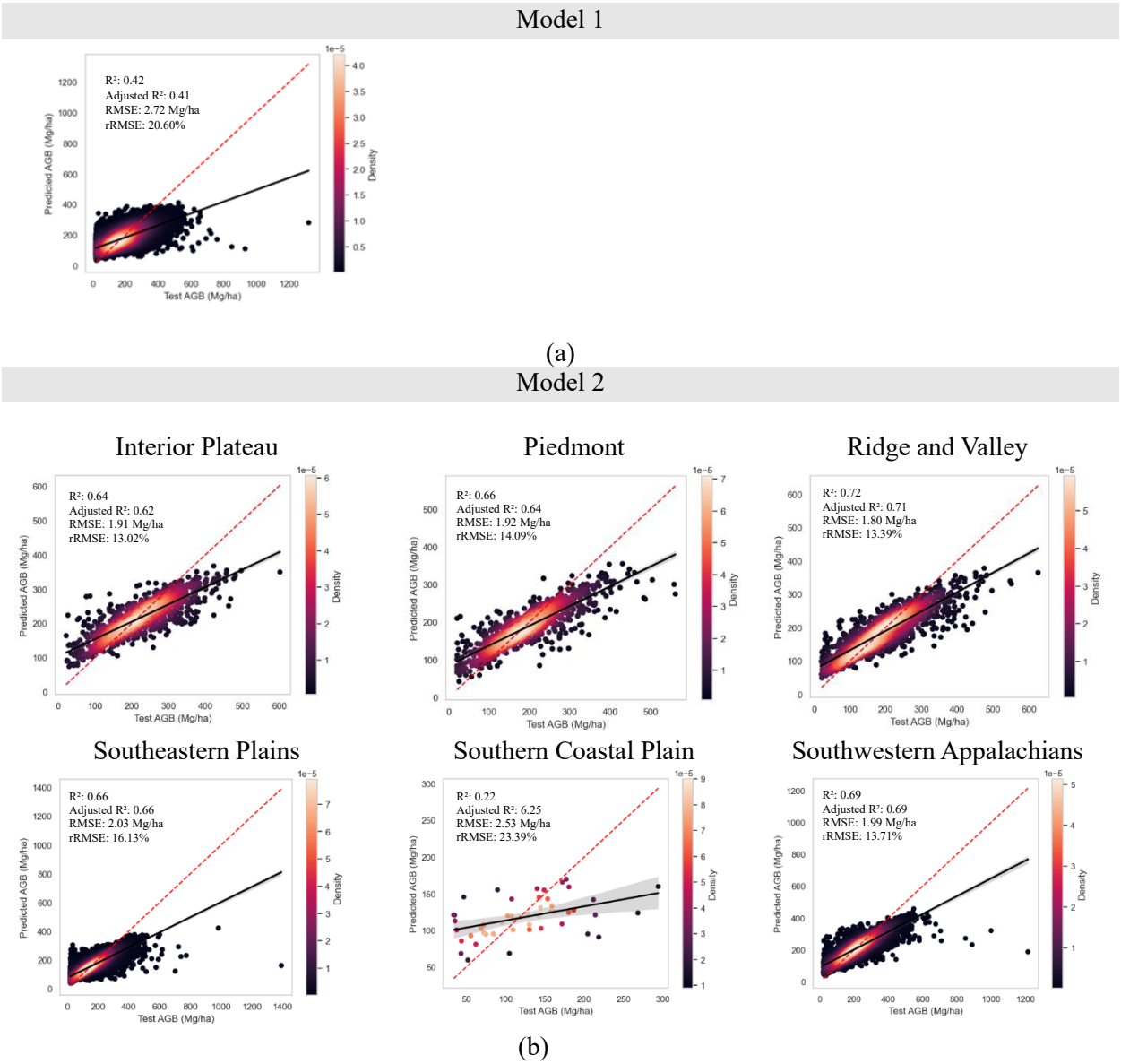


Figure 7. Scatter plot of estimated vs withhold AGBD in Mg/ha (a) performance of Model 1. And (b) performance of Model 2.

The relative variable importance graph highlighted the predictors' effect on model enhancement across the six ecoregions. As in Figure 8 the results revealed that variables from the LANDFIRE program outperformed other predictors, underscoring the significance of LANDFIRE data in AGBD estimation.

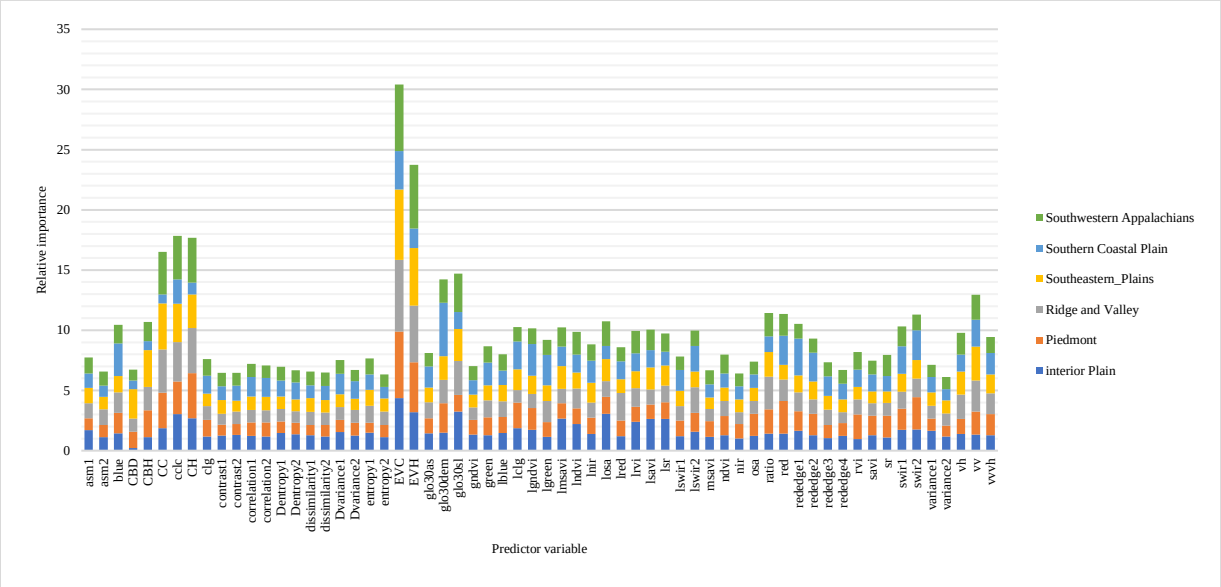


Figure 8. Variable importance at each ecoregion for all 63 predictors

The AGBD estimate map depicted in Figure 9 illustrates the AGB estimation derived from model 2.

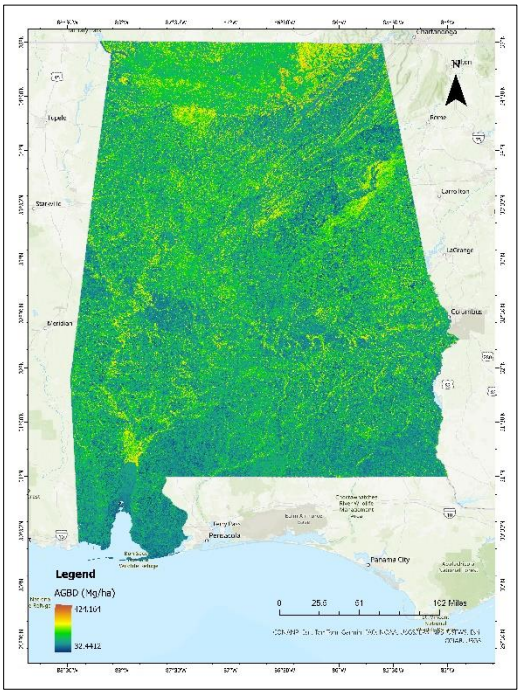


Figure 9. Predicted AGBD at 30 m spatial resolution by Model 2.

### 3.2 Comparison of estimated AGBD with forest inventory data and globally available AGBD product

We aggregated FIA plot data by calculating the average AGBD at the county level to compare with the average AGBD derived from the estimated AGBD in our study. The comparison of mean AGBD between county-aggregated FIA plot data and estimated AGBD yielded an $R^2$ of 0.50, with an RMSE of 33.95 Mg/ha, as illustrated in Figure 10 (a). Furthermore, we conducted a pixel-to-pixel level comparison between the estimated AGBD from our study and the AGBD from CCI product and yielded an accuracy with an $R^2$ of 0.81, and RMSE of 83.12 Mg/ha as depicted in Figure 10 (b).

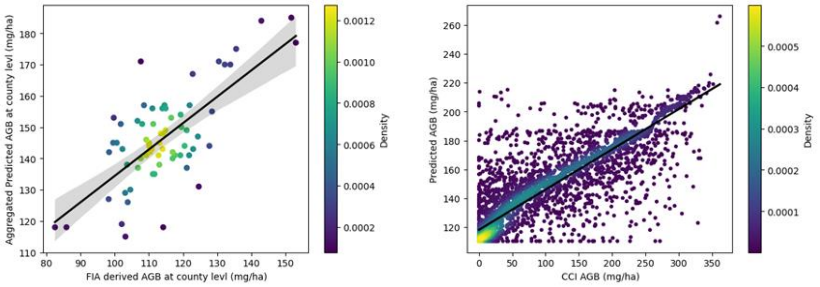


(a) (b)

Figure 10. (a) A scatterplot illustrating the relationship between the mean AGBD at the county level and the AGBD estimated by our study; (b) a pixel-to-pixel level comparison between AGBD derived from the CCI dataset and the estimated AGBD.

### 4. Discussion

We generated a statewide map of AGBD by integrating GEDI L4A and EO data within the GEE platform using RF modeling techniques, achieving a spatial resolution of 30 m. This study underscores the importance of employing an ecoregion-specific approach that is sensitive to the unique conditions within each ecological region. Two modeling approaches were utilized in the study, one considering the entire state as a single entity and the other treating each ecoregion separately, to model and extrapolate AGBD across the study area. Our ecoregion-specific approach demonstrated notable accuracy ($R^2$ of 0.22 - 0.72, and RMSEs of 2.53 Mg/ha - 1.80 Mg/ha) and exhibited generalization capabilities, making it applicable to diverse extents within the studied ecoregions. Studies conducted in forests of the southern US also emphasize the importance of considering a range of variables that capture the high variability of growth patterns in multispecies forests (Brown et al., 2022). Therefore, we incorporated data from a wide range of sources (Table 1) related to forest characteristics, and the utilization of an ecoregion-specific approach allowed us to aggregate similar areas separately, improving prediction accuracy and enhancing the capacity of RF models to handle larger volumes of data. Consequently, we believe our approach can effectively capture the complexity of southern mixed forests in AGBD estimation.

Utilizing a combination of optical, synthetic aperture radar, and lidar data along with ancillary data as predictor variables, we accessed a substantial volume of data for analysis, with the majority of data directly sourced from GEE, obviating the need for manual uploading and processing. This accessibility not only expedites our analytical processes but also capitalizes on GEE's infrastructure, which adeptly manages a larger volume of data through efficient parallel processing across multiple servers. Drawing from the insights of Tamiminia et al. (2022), who utilized a machine learning-based approach within GEE to estimate historical forest AGB in State of New York, our investigation confirms the pivotal role of GEE in AGB estimation. An advantage of the proposed method lies in its reproducibility and shareability facilitated by GEE. Consequently, the entire workflow can be shared for modification aimed at AGB estimation. Therefore, it is suggested utilizing the proposed methodology for assessing annual, seasonal,

or temporal changes in AGBD estimation. In summary, our results emphasize the importance of data accessibility, analysis, and shareability facilitated by cloud computing platforms similar to GEE in advancing future AGB estimation efforts.

Here we implemented various filtering techniques aimed at enhancing the quality of the footprint AGBD, as recommended by prior research (Kellner et al., 2022, Shendryk, 2022). Despite our efforts, we encountered a significant reduction, losing approximately 99% of the data compared to the raw dataset due to the filtering process (Xu et al., 2021). Consequently, augmenting the number of samples for upscaling AGB to ensure greater representativeness and accuracy is suggested. Utilizing data from the ICESat-2 mission offers a promising avenue for enhancing AGBD estimation accuracy, with the potential to increase data density (Guerra-Hernández et al., 2022, Chen et al., 2022, Nandy et al., 2021).

In our analysis, we acknowledged the omission of seasonal fluctuation and climate variability, which could have enriched the accuracy of AGBD estimation. Consequently, future research should incorporate considerations for seasonal fluctuations and climate predictors such as mean annual precipitation, mean annual temperature, as well as seasonal temperature and precipitation variability. Further we are relying solely on median composites of Landsat 9, Sentinel-1, and Sentinel-2 imagery might have generalized the process, potentially leading to information loss crucial for refinement. Hence in future studies we recommend using mean composites as well as considering seasonal attributes when refining EO data for analysis. Additionally, while we exclusively tested RF in this study, we recommend exploring alternative modeling techniques to further enhance the accuracy of AGBD estimation.

The validation of estimated AGBD in our study was conducted through two approaches: comparing field inventory data and global products. Our findings revealed correlations between the FIA data and the ESA CCI AGBD, alongside the AGBD estimated in our study. This validation process provides valuable insights for future remote sensing endeavors, emphasizing discrepancies among biomass products from various platforms. As a result, it emphasizes the urgent need for continued research efforts aimed at improving comprehension and refining methodologies for generating harmonized AGB products.

**Funding**

This work was carried out at the Geospatial Analytics Laboratory at Auburn University in Auburn, Alabama. Research was funded by the USDA Forest Service (Grant # 22-JV-11330180-064).

**Disclosure statement**

The authors report there are no competing interests to declare.

**Data availability statement**

The data used in this study are entirely based on open-access sources and resulting maps are available upon reasonable request to the corresponding author.

**Author information**

Author ORCIDs Janaki Sandamali: //orcid.org/0000-0002-3495-5636

**Author contributions**

Conceptualization: JS, LLN
Writing – JS, LLN

Writing – review & editing: LLN

**5. References**


ADJEI, E., LI, W., NARINE, L. & ZHANG, Y. 2023. What Drives Land Use Change in the Southern U.S.? A Case Study of Alabama. *Forests* [Online], 14.

AFC 2020. FOREST RESOURCE REPORT 2020. Alabama Forestry Commission (ACF).

AGUILAR, F. J., RODRÍGUEZ, F. A., AGUILAR, M. A., NEMMAOUI, A. & ÁLVAREZ-TABOADA, F. 2024. Forestry Applications of Space-Borne LiDAR Sensors: A Worldwide Bibliometric Analysis. *Sensors,* 24**,** 1106.

ARÉVALO, P., BACCINI, A., WOODCOCK, C. E., OLOFSSON, P. & WALKER, W. S. 2023. Continuous mapping of aboveground biomass using Landsat time series. *Remote Sensing of Environment,* 288**,** 113483.

AWF. 2008. *Elementary Ecosystem Investigation: Alabama's Ecoregions* [Online]. ALABAMA WILDLIFE FEDERATION. [Accessed 3.07.2024 2024].

BÉJAR-MARTOS, J. A., RUEDA-RUIZ, A. J., OGAYAR-ANGUITA, C. J., SEGURA-SÁNCHEZ, R. J. & LÓPEZ-RUIZ, A. 2022. Strategies for the Storage of Large LiDAR Datasets—A Performance Comparison. *Remote Sensing,* 14**,** 2623.

BONAN, G. B. 2008. Forests and climate change: forcings, feedbacks, and the climate benefits of forests. *science,* 320**,** 1444-1449.

BOUASRIA, A., BOUSLIHIM, Y., GUPTA, S., TAGHIZADEH-MEHRJARDI, R. & HENGL, T. 2023. Predictive performance of machine learning model with varying sampling designs, sample sizes, and spatial extents. *Ecological Informatics,* 78**,** 102294.

BROWN, S., NARINE, L. L. & GILBERT, J. 2022. Using Airborne Lidar, Multispectral Imagery, and Field Inventory Data to Estimate Basal Area, Volume, and Aboveground Biomass in Heterogeneous Mixed Species Forests: A Case Study in Southern Alabama. *Remote Sensing,* 14.

CAO, G. 2022. Application of Remote Sensing Technology in Forest Resources Investigation. *Remote Sensing,* 11**,** 46-49.

CES 1997. ECOLOGICAL REGIONS OF NORTH AMERICA. *In:* (CEC), C. F. E. C. (ed.). Canada: Commission for Environmental Cooperation.

CHEN, J., CHEN, J., LIAO, A., CAO, X., CHEN, L., CHEN, X., HE, C., HAN, G., PENG, S., LU, M., ZHANG, W., TONG, X. & MILLS, J. 2015. Global land cover mapping at 30m resolution: A POK-based operational approach. *ISPRS Journal of Photogrammetry and Remote Sensing,* 103**,** 7-27.

CHEN, L., REN, C., BAO, G., ZHANG, B., WANG, Z., LIU, M., MAN, W. & LIU, J. 2022. Improved Object-Based Estimation of Forest Aboveground Biomass by Integrating LiDAR Data from GEDI and ICESat-2 with Multi-Sensor Images in a Heterogeneous Mountainous Region. *Remote Sensing,* 14.

CHEN, L., WANG, Y., REN, C., ZHANG, B. & WANG, Z. 2019. Optimal Combination of Predictors and Algorithms for Forest Above-Ground Biomass Mapping from Sentinel and SRTM Data. *Remote Sensing* [Online], 11.

DEWITZ, J. 2023. National Land Cover Database (NLCD) 2021 Products. Earth Resources Observation and Science (EROS) Center.

DUBAYAH, R., ARMSTON, J., HEALEY, S. P., BRUENING, J. M., PATTERSON, P. L., KELLNER, J. R., DUNCANSON, L., SAARELA, S., STÅHL, G., YANG, Z., TANG, H., BLAIR, J. B., FATOYINBO, L., GOETZ, S., HANCOCK, S., HANSEN, M., HOFTON, M., HURTT, G. & LUTHCKE, S. 2022. GEDI launches a new era of biomass inference from space. *Environmental Research Letters,* 17.

DUBAYAH, R., BRYAN, J., GOETZ, S., FATOYINBO, L., HANSEN, M., HEALEY, S., HOFTON, M., HURTT, G., KELLNER, J., LUTHCKE, S., ARMSTON, J., TANG, H., DUNCANSON, L., HANCOCK, S., JANTZ, P., MARSELIS, S., PATTERSON, P. L., QI, W. & SILVA, C. 2020. The

Global Ecosystem Dynamics Investigation : High-resolution laser ranging of the Earth ' s forests and topography. *Science of Remote Sensing,* 1**,** 100002-100002.
DUBAYAH, R. O., J. ARMSTON, J.R. KELLNER, L. DUNCANSON, S.P. HEALEY, P.L. PATTERSON, S. HANCOCK, H. TANG, J. BRUENING, M.A. HOFTON, J.B. BLAIR, AND S.B. LUTHCKE 2022. GEDI L4A Footprint Level Aboveground Biomass Density, Version 2.1. *In:* ORNL DAAC, O. R., TENNESSEE, USA. (ed.).
DUNCAN, R. S. 2013. *Encyclopedia of Alabama* [Online]. Available: https://encyclopediaofalabama.org/article/biodiversity-in-alabama/ [Accessed 01-19 2024].
ESA 2012. Sentinel-1. *In:* FLETCHER, K. (ed.) *Sentinel-1: ESA's Radar Observatory Mission for GMES Operational Services.* Netherlands: European Space Agency.
ESA. 2022. *STEP - Scientific Toolbox Exploitation Platform* [Online]. European Space Agency: European Space Agency. Available: https://step.esa.int/main/snap-supported-plugins/sen2cor/ [Accessed 31.01.2024 2024].
FRANKS, S. & RENGARAJAN, R. 2023. Evaluation of Copernicus DEM and Comparison to the DEM Used for Landsat Collection-2 Processing. *Remote Sensing* [Online], 15.
GORELICK, N., HANCHER, M., DIXON, M., ILYUSHCHENKO, S., THAU, D. & MOORE, R. 2017. Google Earth Engine: Planetary-scale geospatial analysis for everyone. *Remote Sensing of Environment,* 202**,** 18-27.
GUERRA-HERNÁNDEZ, J., NARINE, L. L., PASCUAL, A., GONZALEZ-FERREIRO, E., BOTEQUIM, B., MALAMBO, L., NEUENSCHWANDER, A., POPESCU, S. C. & GODINHO, S. 2022. Aboveground biomass mapping by integrating ICESat-2, SENTINEL-1, SENTINEL-2, ALOS2/PALSAR2, and topographic information in Mediterranean forests. *GIScience and Remote Sensing,* 59**,** 1509-1533.
HARRIS, N. L., GIBBS, D. A., BACCINI, A., BIRDSEY, R. A., DE BRUIN, S., FARINA, M., FATOYINBO, L., HANSEN, M. C., HEROLD, M., HOUGHTON, R. A., POTAPOV, P. V., SUAREZ, D. R., ROMAN-CUESTA, R. M., SAATCHI, S. S., SLAY, C. M., TURUBANOVA, S. A. & TYUKAVINA, A. 2021. Global maps of twenty-first century forest carbon fluxes. *Nature Climate Change,* 11**,** 234-240.
HOLCOMB, A., MATHIS, S. V., COOMES, D. A. & KESHAV, S. 2023. Computational tools for assessing forest recovery with GEDI shots and forest change maps. *Science of Remote Sensing,* 8**,** 100106.
HUMMEL, S., HUDAK, A. T., UEBLER, E. H., FALKOWSKI, M. & MEGOWN, K. 2011. A Comparison of Accuracy and Cost of LiDAR versus Stand Exam Data for Landscape Management on the Malheur National Forest. *Journal of Forestry,* 109**,** 267-273.
JIANG, F., SUN, H., CHEN, E., WANG, T., CAO, Y. & LIU, Q. 2022. Above-Ground Biomass Estimation for Coniferous Forests in Northern China Using Regression Kriging and Landsat 9 Images. *Remote Sensing* [Online], 14.
KACIC, P., HIRNER, A. & DA PONTE, E. 2021. Fusing Sentinel-1 and -2 to Model GEDI-Derived Vegetation Structure Characteristics in GEE for the Paraguayan Chaco. *Remote Sensing,* 13**,** 5105.
KELLNER, J. R., ARMSTON, J. & DUNCANSON, L. 2022. Algorithm theoretical basis document for GEDI footprint aboveground biomass density. *Earth and Space Science,* 10**,** 1-20.
LA PUMA, I. P. 2023. LANDFIRE technical documentation: U.S. Geological Survey Open-File Report 2023–1045, 103 p. *In:* PUMA, A. P. L. (ed.).
LAURIN, G. V., BALLING, J., CORONA, P., MATTIOLI, W., PAPALE, D., PULETTI, N., RIZZO, M., TRUCKENBRODT, J. & URBAN, M. 2018. Above-ground biomass prediction by Sentinel-1 multitemporal data in central Italy with integration of ALOS2 and Sentinel-2 data. *Journal of Applied Remote Sensing,* 12**,** 1-1.
LI, Y., LI, M., LI, C. & LIU, Z. 2020. Forest aboveground biomass estimation using Landsat 8 and Sentinel-1A data with machine learning algorithms. *Scientific Reports,* 10**,** 1-12.

LIU, A., CHENG, X. & CHEN, Z. 2021. Performance evaluation of GEDI and ICESat-2 laser altimeter data for terrain and canopy height retrievals. *Remote Sensing of Environment,* 264**,** 112571.
MADUNDO, S. D., MAUYA, E. W. & KILAWE, C. J. 2023. Comparison of multi-source remote sensing data for estimating and mapping above-ground biomass in the West Usambara tropical montane forests. *Scientific African,* 21**,** e01763.
MALAMBO, L., POPESCU, S. & LIU, M. 2023a. Landsat-Scale Regional Forest Canopy Height Mapping Using ICESat-2 Along-Track Heights: Case Study of Eastern Texas. *Remote Sensing,* 15**,** 1.
MORADI, F., DARVISHSEFAT, A. A., POURRAHMATI, M. R., DELJOUEI, A. & BORZ, S. A. 2022. Estimating Aboveground Biomass in Dense Hyrcanian Forests by the Use of Sentinel-2 Data. *Forests,* 13.
NANDY, S., SRINET, R. & PADALIA, H. 2021. Mapping Forest Height and Aboveground Biomass by Integrating ICESat-2, Sentinel-1 and Sentinel-2 Data Using Random Forest Algorithm in Northwest Himalayan Foothills of India. *Geophysical Research Letters,* 48**,** 1-10.
NARINE, L. L., POPESCU, S. C. & MALAMBO, L. 2019. Synergy of ICESat-2 and landsat for mapping forest aboveground biomass with deep learning. *Remote Sensing,* 11**,** 1-19.
POTAPOV, P., LI, X., HERNANDEZ-SERNA, A., TYUKAVINA, A., HANSEN, M. C., KOMMAREDDY, A., PICKENS, A., TURUBANOVA, S., TANG, H., SILVA, C. E., ARMSTON, J., DUBAYAH, R., BLAIR, J. B. & HOFTON, M. 2021. Mapping global forest canopy height through integration of GEDI and Landsat data. *Remote Sensing of Environment,* 253**,** 112165.
RODRÍGUEZ-VEIGA, P., WHEELER, J., LOUIS, V., TANSEY, K. & BALZTER, H. 2017. Quantifying Forest Biomass Carbon Stocks From Space. *Current Forestry Reports,* 3**,** 1-18.
ROLLINS, M. G. 2009. LANDFIRE: a nationally consistent vegetation, wildland fire, and fuel assessment. *International Journal of Wildland Fire,* 18**,** 235-249.
SHENDRYK, Y. 2022. Fusing GEDI with earth observation data for large area aboveground biomass mapping. *International Journal of Applied Earth Observation and Geoinformation,* 115**,** 103108-103108.
SHEPHARD, N. T., NARINE, L., PENG, Y. & MAGGARD, A. 2022. Climate Smart Forestry in the Southern United States. *Forests* [Online], 13.
SOUDANI, K., DELPIERRE, N., BERVEILLER, D., HMIMINA, G., VINCENT, G., MORFIN, A. & DUFRÊNE, É. 2021. Potential of C-band Synthetic Aperture Radar Sentinel-1 time-series for the monitoring of phenological cycles in a deciduous forest. *International Journal of Applied Earth Observation and Geoinformation,* 104**,** 102505.
TAMIMINIA, H., SALEHI, B., MAHDIANPARI, M., BEIER, C. M. & JOHNSON, L. 2022. Mapping Two Decades of New York State Forest Aboveground Biomass Change Using Remote Sensing. *Remote Sensing* [Online], 14.
TIWARI, K. & NARINE, L. L. 2022. A Comparison of Machine Learning and Geostatistical Approaches for Mapping Forest Canopy Height over the Southeastern US Using ICESat-2. *Remote Sensing,* 14.
USFWI. 2024. *Alabama Butterfly Atlas* [Online]. USF Water Institute: University of South Florida. [Accessed].
XU, L., YANG, Y. & SAATCHI, S. Sampling accuracy and data filtering of GEDI data in the tropical rainforest regions. AGU Fall Meeting Abstracts, 2021. B45H-1715.
YANG, Q., NIU, C., LIU, X., FENG, Y., MA, Q., WANG, X., TANG, H. & GUO, Q. 2023. Mapping high-resolution forest aboveground biomass of China using multisource remote sensing data. *GIScience & Remote Sensing,* 60**,** 2203303.